Hindawi
Scientific Programming
Volume 2021, Article ID 8210526, 9 pages
https://doi.org/10.1155/2021/8210526

Research Article

Improved Quantitative Susceptibility Mapping under Laplace Algorithm in Diagnosis of Parkinson's Disease

Guangxi Chen,[1] **Liang Zeng**,[2] **Liu Yang**,[1] **Yixian Yu**,[1] **Panli Sun**,[1] **and Tao Yao**[1]

[1]*Department of Neurology, Wuhan Third Hospital, Tongren Hospital of Wuhan University, Wuhan 430060, Hubei, China*
[2]*Department of Geriatrics, China Resources & WISCO General Hospital, Affiliated to Wuhan University of Science and Technology, Wuhan 430080, Hubei, China*

Correspondence should be addressed to Tao Yao; 17071010210017@hainanu.edu.cn

Received 30 August 2021; Revised 24 October 2021; Accepted 25 October 2021; Published 12 November 2021

Academic Editor: Gustavo Ramirez

To explore the application value of quantitative susceptibility mapping (QSM) based on Laplace algorithm in the diagnosis of Parkinson's disease, 48 Parkinson's disease patients admitted to our hospital were included as the research objects. They were randomly divided into control group (24 cases) and experimental group (24 cases). All patients underwent quantitative magnetic susceptibility imaging scan. In the experimental group, the improved Laplace algorithm was used for QSM diagnosis, while in the control group, conventional QSM diagnosis was used. Through calculations of precision, recall, dice similarity coefficient, intersection-over-union (IoU), and area under the curve (AUC), the quality improvement effect of the improved Laplace algorithm for QSM image was assessed. Then, the diagnostic accuracy of the algorithm was verified by comparing with the results of QSM image diagnosis in Parkinson's patients without algorithm processing. The results showed that compared with the traditional Laplace algorithm, the improved Laplace algorithm can considerably reduce the image noise level ($P < 0.05$). The dice, IoU, precision, and recall rate of image quality evaluation indicator were considerably improved ($P < 0.05$), and the AUC reached 0.896. There were no significant differences in fraction anisotropy (FA) and mean diffusivity (MD) between the two groups ($P > 0.05$) and no significant differences in magnetic susceptibility of brain nuclei between the two groups ($P > 0.05$). However, they all showed high magnetic susceptibility in the substantia nigra region of the brain. Compared with the control group, the diagnostic accuracy of the experimental group was $97.5 \pm 1.23\%$, which was considerably higher than that of the control group ($86.5 \pm 3.56\%$) ($P < 0.05$). In short, the image quality of QSM based on Laplace improved algorithm was greatly improved, and the diagnostic accuracy of PD was also greatly improved, which was worthy of promotion in the field of clinical QSM imaging diagnosis of PD.

1. Introduction

Parkinson's disease (PD), also known as palsy tremor, is a neurodegenerative disease common in middle-aged and elderly people. Clinically, static tremor, bradykinesia, myotonia, and postural balance disorders are the main characteristics. In addition, it may be accompanied by sensory disorders, sleep disorders, and autonomic nervous dysfunction [1–3]. The main pathological change of this disease is the degeneration and death of dopaminergic neurons in the substantia nigra, but the etiology and pathogenesis of the degeneration and death of dopaminergic neurons in the substantia nigra have not yet been fully clarified [4]. Due to the insidious onset and slow progress of the disease, it is necessary to carry out timely and effective early diagnosis. In case of involuntary trembling, muscle stiffness, slow movement, and other symptoms when limbs are still, medical treatment should be sought in time [5]. Routine clinical examinations include blood routine, routine cerebral effusion, CT and MRI, positron emission tomography (PET) or single photon emission computed tomography (SPECT), transcranial ultrasound (TCS), and quantitative susceptibility mapping (QSM) [6, 7]. QSM is a technology for quantitatively measuring the susceptibility of tissues, which is developed from the magnetism sensitive weighted imaging (SWI) [8]. This technique obtains the

change of tissue magnetic field from the phase information and then obtains the value of magnetic susceptibility through inverse calculation [9]. Magnetic susceptibility reflects the change of tissue composition by reflecting the degree of magnetization of biological tissue in the external magnetic field. Among them, diamagnetic substances, such as calcification and fat, have negative susceptibility, while paramagnetic substances, such as deoxyhemoglobin and hemosiderin have, positive susceptibility [10]. QSM can describe the distribution of magnetic susceptibility in the imaging site, thus indirectly reflecting the content of iron in the body, blood vessels, and tissue structure. It is a good method for the diagnosis and research of PD [11, 12]. At present, QSM relies on phase information to measure the magnetic characteristics of tissues and has been successfully applied to the measurement of iron deposition, blood oxygen saturation, differentiation of bleeding, and calcification. [13]. However, QSM currently has problems such as phase artifact interference, and region of interest (ROI) need to be manually drawn, which wastes time and has errors [14].

Laplace image enhancement algorithm is a second-order differential algorithm in the spatial domain, which can extract the edge information of the image by highlighting the fuzzy details, so as to present a clearer visual effect. This algorithm has low requirements on hardware and strong practicability and has been widely utilized in many fields at present [15, 16]. Therefore, Laplace algorithm was combined with QSM in this research to design a QSM image processing method based on improved Laplace algorithm, which was applied to the clinical diagnosis of PD patients. The adoption potential of QSM based on improved Laplace algorithm in the diagnosis of PD was comprehensively evaluated by comparing the diagnosis of PD patients in the experimental group without improved Laplace algorithm.

2. Materials and Methods

2.1. Research Objects. In this study, 48 Parkinson's patients admitted to the hospital were selected as the research subjects, including 24 males and 24 females, aged 45–71 years, with a mean age of 65.3 ± 2.3 years. All subjects were randomly divided into experimental group and control group, with 24 patients in each group. Quantitative susceptibility imaging scans were then performed on all subjects. The experimental group performed quantitative susceptibility imaging based on the improved Laplace algorithm for diagnosis. The control group was diagnosed by only quantitative magnetic susceptibility imaging.

The inclusion criteria for Parkinson's disease patients included the following: (i) those who met the diagnostic criteria of "Chinese Parkinson's Disease Diagnostic Criteria (2016 Edition);" (ii) those over 18 years old; (iii) all patients signing an informed consent form and agreeing to undergo SWI, R2 $*$, MRF, and QSM3.0T magnetic resonance examinations; (iv) complete medical history information.

The exclusion criteria included the following: (i) the patient had various contraindications to MRI, such as metal implantation; (ii) patients suffering from claustrophobia; (iii) unqualified image quality of quantitative magnetization imaging due to various reasons; (iv) patients with a history of various neurological diseases, such as schizophrenia and bipolar disorder; (v) patients with neurodegenerative diseases, epilepsy, brain tumors, ischemic or hemorrhagic stroke, hydrocephalus, multiple sclerosis, and other diseases; (vi) patients with a history of other brain surgery or deep brain stimulation.

The ethics committee of the hospital approved the study, and the enrolled patients and their families signed informed consent.

2.2. Parameters Related to QSM. In this study, Trio Tim (Siemens) was utilized to collect the QSM pattern, phase, and DTI raw data, and the 3D multiecho gradient echo sequence was utilized for QSM scanning. The relevant parameter information is shown in Table 1.

2.3. Laplace Algorithm Improvement. The Laplace image enhancement algorithm utilized in this research is a kind of isotropic filtering algorithm, which is an algorithm that enhances the image through second-order differentiation. The response of the filter in this algorithm is not directly related to the sudden change of the image being acted upon. Because of its low hardware requirements and simple operation, it has been widely utilized in image intensifier high-frequency enhancement algorithms. The restricted Laplace enhancement algorithm utilized in this study improved the effect of noise processing based on the ordinary Laplace enhancement algorithm. When this algorithm is used, a two-dimensional continuous function $S(a,b)$ is first defined, and a two-dimensional column vector is utilized to express the gradient of the point as follows:

$$\overline{H}[S(a,b)] = \begin{bmatrix} \dfrac{\partial S}{\partial a} \\ \\ \dfrac{\partial S}{\partial b} \end{bmatrix}. \tag{1}$$

The partial derivative of a at (a,b) is expressed as follows:

$$\frac{\partial S}{\partial a} = \lim_{\varepsilon \longrightarrow 0} \frac{S(a+\varepsilon,b) - s(a,b)}{\varepsilon}. \tag{2}$$

The partial derivative of b at (a,b) is expressed as follows:

$$\frac{\partial S}{\partial b} = \lim_{\varepsilon \longrightarrow 0} \frac{S(a,b+\varepsilon) - s(a,b)}{\varepsilon}. \tag{3}$$

The magnitude of the gradient is utilized to express the maximum rate of change of the function $S(a,b)$, and its calculation is as follows:

$$H(S(a,b)) = \sqrt{\left(\frac{\partial S}{\partial a}\right)^2 + \left(\frac{\partial S}{\partial b}\right)^2}. \tag{4}$$

In digital images, image data is represented by a discontinuous discrete matrix. The gradient of each pixel is

Table 1: Parameter information.

Parameter item	Value
Repeat time	60 ms
First echo time	6.78 ms
Echo interval time	6.5 ms
Number of echoes	8
Flip angle	15°
Parameter	Reference
Repeat time	60 ms
Vision	240 mm × 18 mm
Matrix size	380 × 290
Voxel size	0.5 mm × 0.5 mm × 2
Number of layers	96
Sampling bandwidth	240 Hz/pixel
Parallel imaging acceleration factor	2

approximated by the difference between the center pixel and the neighboring pixels. The calculation is as follows:

$$H(S(p,q)) = \sqrt{(S(p,q) - S(p+1,q))^2 + (S(p,q) - S(p,q+1))^2}. \tag{5}$$

In (5), p and q are integers, $S(p,q)$ represents the pixel value at the coordinate. To simplify the algorithm in actual operation, the previously mentioned equation is simplified to

$$H(S(p,q)) = |H_p| + |H_q|. \tag{6}$$

The simplified equation (6) is expanded to

$$H(S(p,q)) = |S(p,q) - S(p+1,q)| + |S(p,q) - S(p,q+1)|. \tag{7}$$

The simplified gradient algorithm in (7) is expressed by the horizontal and vertical difference operator. This method can only effectively detect the edges in the horizontal direction and the vertical direction and has a weak processing capability for the edges of the image with a certain inclination angle. On this basis, the Robert cross operator is introduced, which can detect the difference of the oblique component very well, and its calculation is expressed as follows:

$$\begin{aligned} H(S(p,q)) = {} & |S(p+1,q+1) - S(p,q)| \\ & + |S(p+1,q) - S(p,q+1)|. \end{aligned} \tag{8}$$

The Robert operator mentioned in (8) belongs to the first-order differential operator. Then, the Laplace operator of the second-order differential is introduced. This operator has isotropy and unique invariance. This operator belongs to the second-order differential operator, and its calculation is expressed as follows:

$$\nabla^2(S(a,b)) = \frac{\partial^2 S}{\partial a^2} + \frac{\partial^2 S}{\partial b^2}. \tag{9}$$

Since the digital information of the quantitative magnetization imaging of PD patients to be processed is in the form of discrete points, the previously mentioned second-order differential equation is replaced by a difference equation, and the obtained first-order partial derivative equation is expressed as follows:

$$\begin{cases} \dfrac{\partial S(p,q)}{\partial a} = S(p,q) - S(p-1,q), \\ \dfrac{\partial S(p,q)}{\partial b} = S(p,q) - S(p,q-1). \end{cases} \tag{10}$$

The second-order partial derivative equation is expressed as follows:

$$\begin{cases} \dfrac{\partial^2 S(p,q)}{\partial a^2} = |S(p+1,q) - S(p,q)| + |S(p-1,q) - S(p,q)|, \\ \dfrac{\partial^2 S(p,q)}{\partial b^2} = |S(p,q+1) - S(p,q)| + |S(p,q-1) - S(p,q)|. \end{cases} \tag{11}$$

From the previously mentioned equation, the discrete expression of Laplace is obtained and expressed as follows:

$$\begin{aligned} \nabla^2(S(a,b)) &= \frac{\partial^2 S}{\partial a^2} + \frac{\partial^2 S}{\partial b^2} \\ &= |S(p-1,q) + S(p+1,q) \\ &\quad + S(p,q-1) - 4 * S(p,q)|. \end{aligned} \tag{12}$$

To alleviate the image blur problem caused by the diffusion phenomenon, an enhancement function is introduced, as shown in

$$h(p,q) = S(p,q) - g * \nabla^2 S(a,b). \tag{13}$$

In (13), k represents the correlation coefficient of the diffusion effect, and its value directly affects the enhancement effect of the image. When the k value is too large, the edge of the image will appear overshooting, and when the k value is too small, the edge extraction effect of the image will be poor. It is assumed that $k = 1$, and the obtained image enhancement equation is expressed as

$$\begin{aligned} h(p,q) = {} & 5 * S(p,q) - S(p+1,q) - S(p-1,q) \\ & - S(p,q+1) - S(p,q-1). \end{aligned} \tag{14}$$

Another Laplace enhancement template, the eight-neighbor enhancement template, is introduced to enhance the image enhancement effect. The model diagram is shown in Figure 1. The enhancement equation of the template is expressed as follows:

$$\begin{aligned} h(p,q) = {} & 9 * S(p,q) - S(p+1,q) - S(p-1,q) \\ & - S(p,q+1) - S(p,q-1) \\ & - S(p-1,q-1) - S(p-1,q+1) \\ & - S(p+1,q-1) - S(p+1,q+1). \end{aligned} \tag{15}$$

The eight-neighbor enhancement Laplace enhancement algorithm can effectively extract the edge information of the image while amplifying the noise of the image to a large

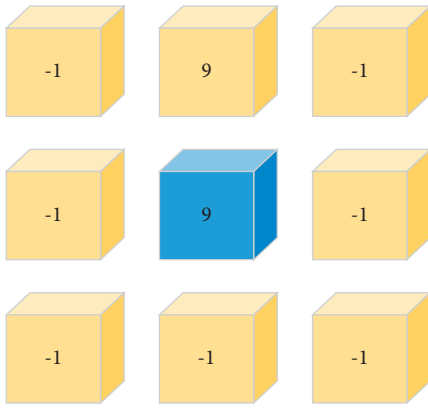

Figure 1: Eight-neighbor Laplace enhanced template.

extent. To solve this problem, a restricted Laplace enhancement algorithm is introduced, which can determine the contrast between the center pixel and the pixel value of the neighborhood by setting a threshold. If the contrast is large, the image is not enhanced. If the contrast is small, the enhanced value is taken as the central pixel value. The calculation of its contrast is expressed as follows:

$$\delta = \frac{T_{\max} - T_{\min}}{T_{\max} + T_{\min}}. \tag{16}$$

The expression of $T_{\max}, T_{\min}$ in (16) is as follows:

$$\begin{aligned} T_{\min} &= \min(v11, v12, v13, v21, v22, v23, v31, v32, v33), \\ T_{\max} &= \max(v11, v12, v13, v21, v22, v23, v31, v32, v33). \end{aligned} \tag{17}$$

The restricted Laplace enhancement equation is expressed as follows:

$$H' = \begin{cases} v22, & \delta \geq 0.5, \\ H, & \delta < 0.5. \end{cases} \tag{18}$$

The contrast is introduced into the restricted Laplace enhancement equation. When $\delta \geq 0.5$, the pixel is not enhanced, and the center pixel is retained. When $\delta < 0.5$, the pixel is enhanced by the Laplace algorithm.

2.4. QSM Laplace Algorithm Optimization and Algorithm Evaluation Indicators. The QSM reconstruction algorithm is utilized in the field of accurate segmentation of traditional QSM images. The algorithm segmented QSM images through image preprocessing, background field removal, and magnetic susceptibility inversion. When multiecho gradient imaging is performed to acquire a QSM image sequence, the nonlinear least squares equation is utilized to express the fitted magnetic field map. The equation is expressed as follows:

$$W(c) = \arg\min_{W(c)} \sum_{l=1}^{M_i} \left\| z(c, QP_l) - d(c, QP_l) e^{-rcF_0 W(c) QP_l} \right\|_2^2. \tag{19}$$

In background field removal, due to the different adoption scenarios of different background field removal algorithms, the artifact removal method based on the complex harmonic theory is adopted to remove the background field and then remove the background field from the image to get the local field of interest. A relatively accurate brain magnetic susceptibility distribution is obtained by calculating the physical relationship between this area and the magnetic susceptibility. It is assumed that there is a given magnetic field Y_0, the normalized phase is denoted by $\psi = (\Phi/\gamma\mu_0 Y_0)$, and Φ represents the measured phase under a given condition, and then, the magnetic susceptibility equation can be expressed as follows:

$$\psi = F^{-1}\{B_2 \cdot F\{\chi\}\}. \tag{20}$$

In (20), F represents the Fourier transform, B represents the magnetic dipole convolution kernel, and its calculation equation is expressed as follows:

$$B_2 = F\left\{ \frac{\Delta c_e \Delta c_f \Delta c_g \left[3(K \cdot c)^2 - \left(c_e^2 + c_f^2 + c_g^2\right)\right]}{4\pi\left(c_e^2 + c_f^2 + c_g^2\right)^{5/2}} \right\}. \tag{21}$$

In (21), c represents the vector position, K represents the applied magnetic field vector, c_e, c_f, c_g are the space coordinates, $\Delta c_e, \Delta c_f, \Delta c_g$ are the voxel sizes, and the unknown magnetic susceptibility map is expressed by

$$\chi = \min\left\{ \left\| F^{-1}\{B_2 \cdot F\{\chi\}\} - \psi \right\|_2 + \lambda \| U \cdot V \cdot \chi \|_1 \right\}. \tag{22}$$

In (22), ψ is the normalized phase of the removed background field, λ is the weighting parameter, and the L_1 norm expression is expressed as follows:

$$\| U \cdot V \cdot \chi \|_1 = \sqrt{\left(U_{Ve} V_e \chi\right)^2 + \left(U_{Vf} V_f \chi\right)^2 + \left(U_{Vg} V_g \chi\right)^2}. \tag{23}$$

In (23), V_e, V_f, and V_g are gradient operators, and U_{Ve}, U_{Vf}, and U_{Vg} are brain tissue weighting coefficients.

Through the previously mentioned algorithm, the QSM images of PD patients in the experimental group were processed, and the QSM of the patients after the treatment was analyzed to compare the diagnostic effect with the control group.

2.5. Evaluation of QSW Image Segmentation Effect Based on Improved Laplace Algorithm. To measure the pros and cons of the algorithm, the precision and recall in pixels were taken as evaluation indicators. The dice similarity coefficient and the intersection-over-union (IoU) with the region as the measurement unit were utilized as the evaluation indicators for the segmentation of the QSM image of the brain of PD patients. Precision is also called the precision rate, which reflects the accuracy of segmentation, and its expression is shown in (24). Recall rate, also known as sensitivity, represents the proportion of positive samples in the prediction results, and its expression is shown in (25). The dice similarity coefficient is a measure of the overlap between the

segmentation result and the gold standard area, and its expression is shown in (26). IoU reflects the degree of coincidence between the real result and the predicted result, and its expression is shown in (27).

$$\text{precision} = \frac{A \cap B}{A} \times 100\%, \tag{24}$$

$$\text{Recall} = \frac{A \cap B}{B} \times 100\%, \tag{25}$$

$$\text{Dice}(A, B) = 2 \times \frac{A \cap B}{A + B}, \tag{26}$$

$$\text{IoU} = \frac{A \cap B}{A \cup B}. \tag{27}$$

In the previously mentioned equations, A represents the standard value segmented by the doctor, and B represents the predicted value segmented by the improved Laplace algorithm. The smaller the dice coefficient, the larger the differences between the predicted result and the real result. The receiver operating characteristic curve (ROC) was utilized to calculate the area under the curve (AUC) of the two algorithms to compare the stability of the algorithm quality changes.

2.6. Comparison of Results of Improved QSM Diagnosis of PD Based on Laplace Algorithm. The magnetic susceptibility of brain nuclei in patients with QSM images of the experimental group and the control group was compared. The measured areas included substantia nigra, red nucleus, caudate nucleus, globus pallidus, putamen, thalamus, and white matter. Anisotropy score (FA) and mean diffusion coefficient (MD) of the two groups were measured. Then, the diagnostic accuracy was calculated according to the diagnostic results of the two groups.

2.7. Statistical Methods. SPSS 19.0 was employed for data statistics and analysis. Mean ± standard deviation ($\overline{x} \pm s$) was how measurement data were expressed, and t test was utilized to compare the mean values among all groups. Statistical data were expressed as percentage (%), and χ^2 test was used. $P < 0.05$ was utilized to indicate statistically remarkable differences.

3. Results

3.1. Comparison of the Noise Level of Patients' QSM Images before and after the Improvement of Laplace Algorithm. Figure 2 shows the comparison of the noise level of each nucleus in the QSM image processed by the conventional Laplace algorithm and the improved Laplace algorithm. The results showed that the noise level of each nucleus of the QSM image was reduced to a certain extent after the improved Laplace algorithm was processed compared with the conventional Laplace algorithm. The noise level of substantia nigra, red nucleus, and globus pallidus was considerably different ($P < 0.05$). However, the noise level of caudate nucleus and putamen was not considerably different between the two algorithms ($P > 0.05$).

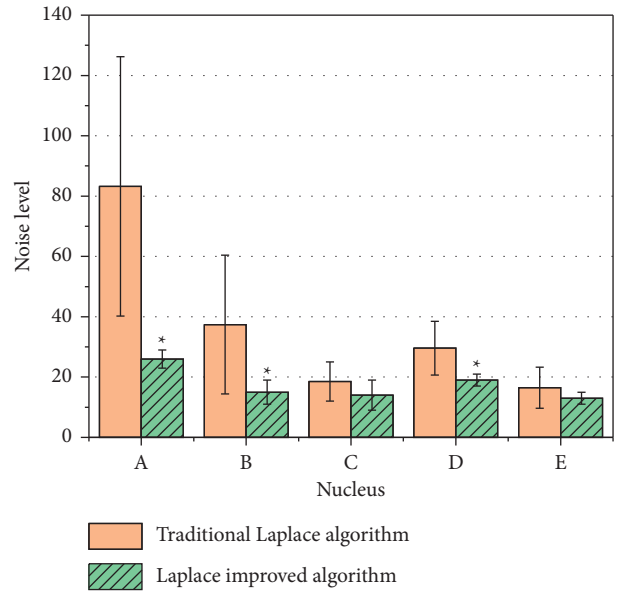

Figure 2: Comparison of the noise level of the core group in the QSM image of the two algorithms. (A) Substantia nigra; (B) red nucleus; (C) caudate nucleus; (D) globus pallidus; (E) putamen; *indicates a remarkable difference compared with the control group ($P < 0.05$).

3.2. Comparison of QSM Image Enhancement Effect of Patients before and after Being Processed by Laplace Algorithm. Figure 3 shows the comparison of QSM images of a 68-year-old male patient before and after being processed with improved Laplace algorithm. Compared with the QSM image that were not processed by the Laplace algorithm, the quality of QSM images processed by the conventional Laplace algorithm and the improved Laplace algorithm was considerably improved, and the sharpness of brain edges was greatly improved.

3.3. QSM Image Quality Assessment Based on Improved Laplace Algorithm. Figure 4 shows the comparison diagram of the quantification of the QSW image processing effect of the traditional Laplace algorithm and the improved Laplace algorithm on PD patients. The indicators included accuracy, recall rate, dice coefficient, and IoU. The precision, recall rate, dice coefficient, and IoU of the improved Laplace algorithm were higher than those of the traditional Laplace algorithm, and the difference was substantial ($P < 0.05$). Figure 5 shows the comparison chart of AUC between the traditional Laplace algorithm and the improved Laplace algorithm. The AUC of the traditional Laplace algorithm was 0.78, and that of the improved Laplace algorithm was 0.896.

3.4. Comparison of the Diagnosis Results of QSM of PD Patients between the Two Groups. Figure 6 is a comparison chart of the magnetic susceptibility of each nucleus in the QSM

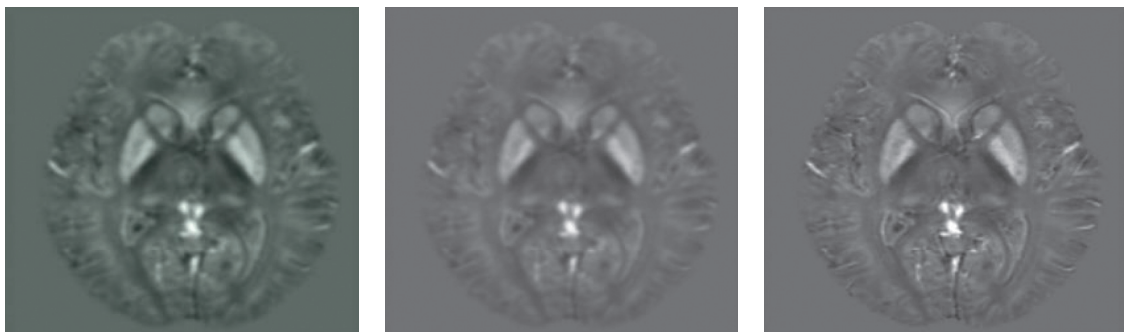

(a) (b) (c)

Figure 3: QSM images of a 68-year-old male patient. (a) Conventional QSM image; (b) QSW image processed by the traditional Laplace algorithm; (c) QSM image processed by the improved Laplace algorithm.

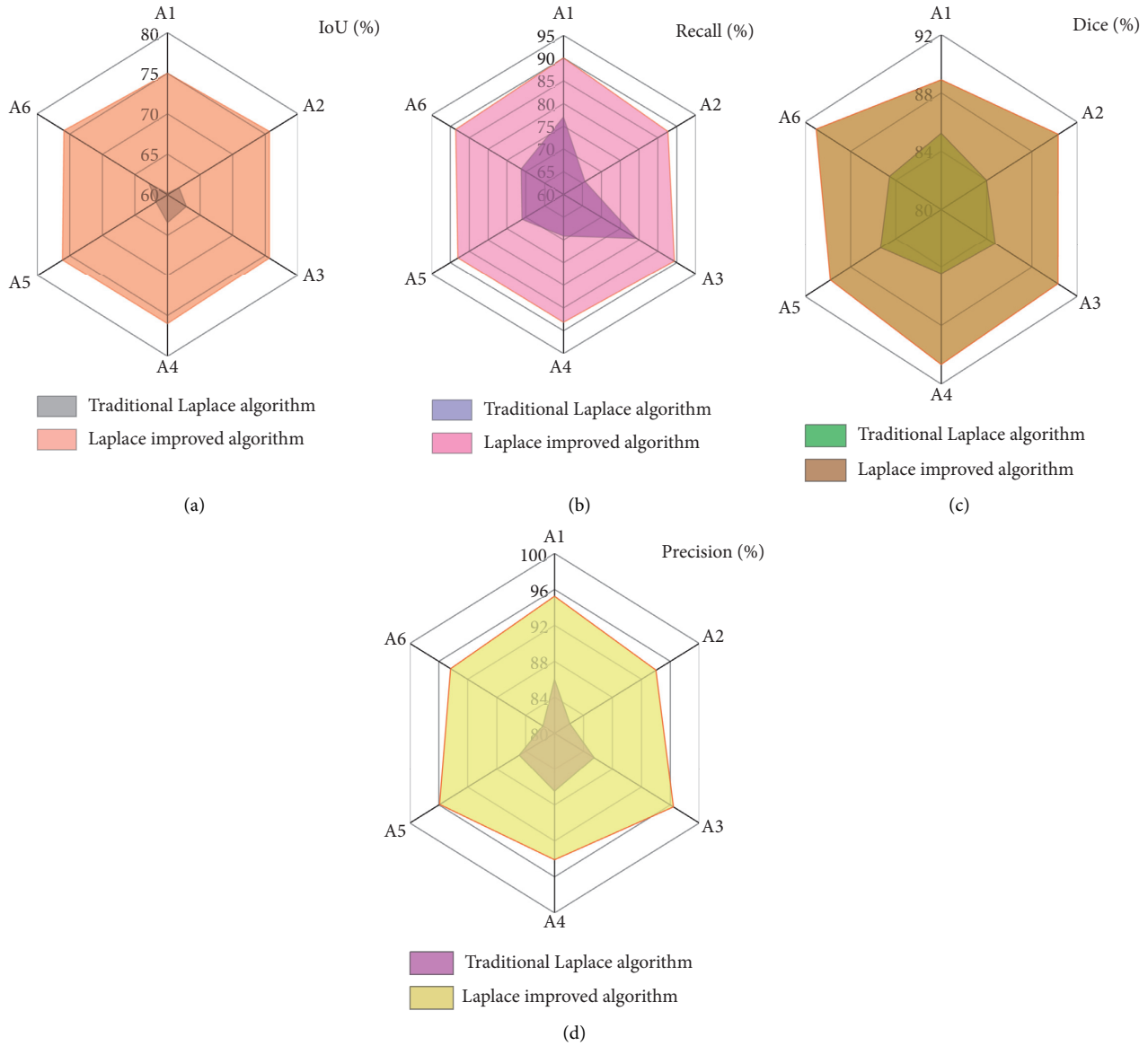

Figure 4: Comparison of image quality evaluation indicators of the two algorithms (A1, A2, A3, A4, A5, and A6 represent the trial numbers of multiple image optimization tests based on algorithms, resp.).

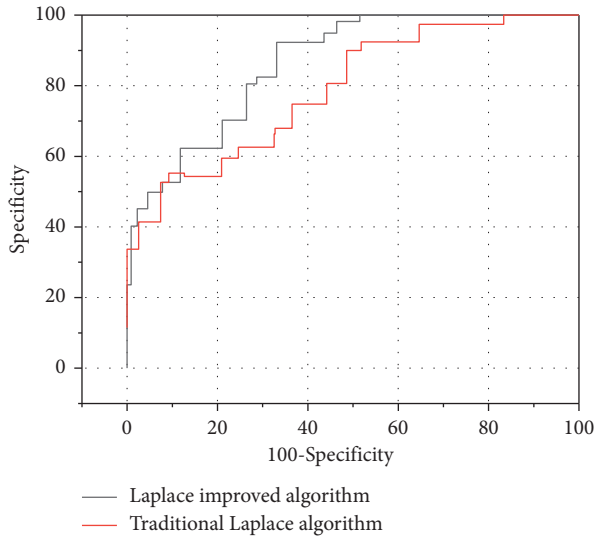

Figure 5: Comparison of AUC of the two algorithms.

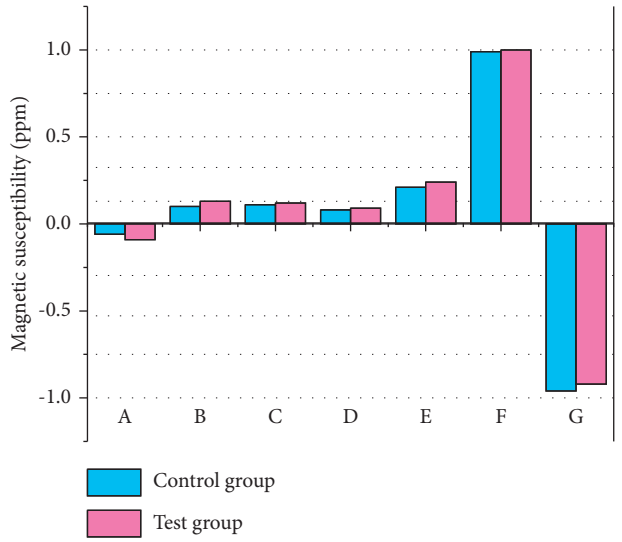

Figure 6: Comparison of magnetic susceptibility of each nucleus in QSM images of two groups of patients. (A) White matter; (B) caudate nucleus; (C) putamen; (D) thalamus; (F) globus pallidus; (E) substantia nigra; (G) calcification point.

images of the two groups of patients. Figure 6 shows that the magnetic susceptibility values of the white matter and calcification points in the QSM images of the two groups of patients were less than 0, while the magnetic susceptibility values of the caudate nucleus, putamen, thalamus, globus pallidus, and substantia nigra were all greater than 0. Among them, the magnetic susceptibility of the substantia nigra region was the highest, reaching 0.99 ppm in the experimental group and 1 ppm in the control group. However, the difference between the magnetic susceptibilities of each nucleus between the two groups was not significant ($P > 0.05$). Figure 7 shows the comparison of the FA and MD values of the magnetic susceptibility of each nucleus in the two sets of QSM images. Figure 7 shows that the FA and MD

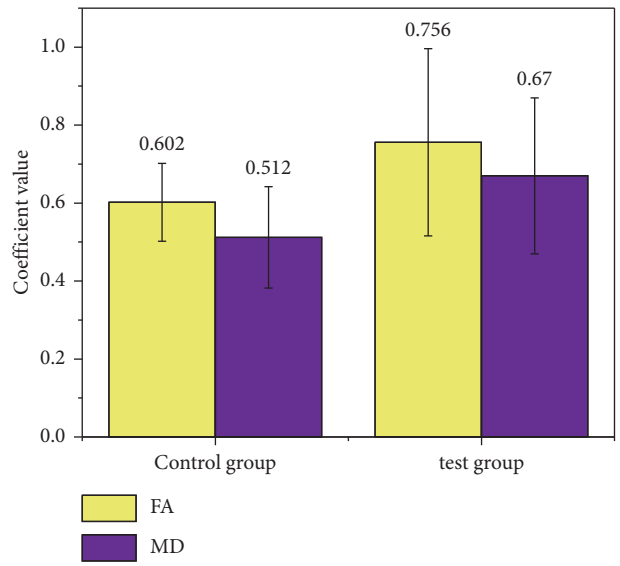

Figure 7: Comparison of FA and MD values of magnetic susceptibility of each nucleus in the two sets of QSM images.

values of the control group were 0.602 ± 0.1 and 0.512 ± 0.13, respectively, and the FA and MD values of the experimental group were 0.756 ± 0.24 and 0.67 ± 0.2, respectively. The difference in FA and MD values between the two groups was not significant ($P > 0.05$). Figure 8 is a comparison chart of the diagnosis accuracy of Parkinson's disease between the two groups of patients. The diagnostic accuracy of the experimental group reached $97.5 \pm 1.23\%$, which was significantly greater than the $86.5 \pm 3.56\%$ of the control group ($P < 0.05$).

4. Discussion

Currently, the gold standard for the diagnosis of PD is Lewy's pathology and SNpc degeneration [17]. It was revealed that because iron deposition in the substantia nigra of the brain affects the abnormal accumulation of alpha-synuclein in Lewy's pathology, iron deposition in the substantia nigra of the brain has become one of the diagnostic markers of PD [18]. QSM technique has been widely utilized in the diagnosis of PD in recent years for it can well show the iron deposition in the substantia nigra in the brain of patients with PD [19]. Currently, the preoperative diagnosis of PD using QSM technique has been widely adopted. The advantage of QSM is that it can quantify the volume susceptibility in the voxel, show the real shape and size of the iron-containing source, and distinguish diamagnetic calcification and paramagnetic iron. However, there are still problems in the clinical adoption of QSM, such as unstable image quality and misdiagnosis in the traditional discriminant method of physicians [20]. Therefore, it is very necessary to improve the overall quality of QSM images and reduce the difficulty of QSM image screening.

To sum up, Laplace algorithm and QSM were combined for QSM image enhancement and automatic segmentation. By comparing the results with the traditional QSM image diagnosis results of the control group, the adoption potential

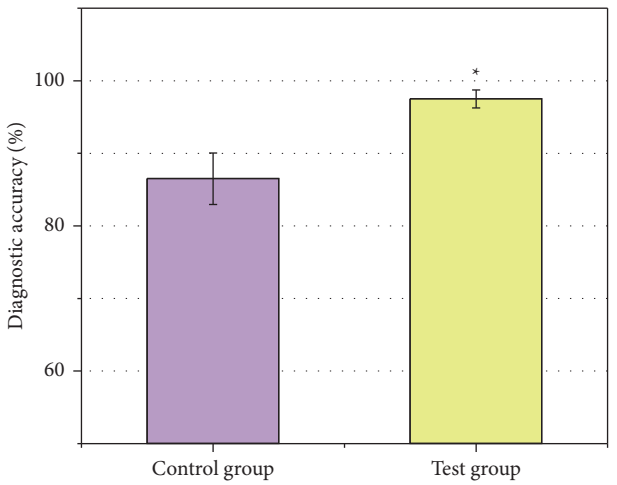

Figure 8: Comparison of the diagnostic accuracy of PD between the two groups (* means remarkable difference compared with the control group ($P < 0.05$)).

of the proposed algorithm in the QSM image diagnosis of PD was comprehensively evaluated. The results showed that compared with the traditional Laplace algorithm, the improved Laplace algorithm can considerably reduce the image noise level ($P < 0.05$). The dice, IoU, precision, and recall rate of image quality evaluation indicators were considerably improved, with substantial differences ($P < 0.05$), and the AUC value reached 0.896. The results indicated that the proposed algorithm can effectively improve the processing effect of QSM image and increase the contrast of the focal area of PD through region enhancement processing, so as to better and faster disease diagnosis. Compared with the diagnosis of the control group, it was found that there was no significant difference in the FA value and MD value of the two groups of patients ($P > 0.05$). There was no significant difference in the magnetic susceptibility of the brain nuclei of the two groups of patients ($P > 0.05$), but the substantia nigra region of the brain showed a high level of magnetic susceptibility ($P < 0.05$). Compared with the control group, the diagnostic accuracy of the experimental group was considerably improved ($P < 0.05$). It was suggested that the proposed algorithm can improve the efficiency of QSM imaging diagnosis of PD and provide a theoretical and practical basis for the research of improving the quality of QSM imaging diagnosis of PD. Similarly, the study by Zou et al. [20] pointed out that multiscale image reconstruction can be achieved by constructing an image super-resolution reconstruction algorithm based on the Laplace pyramid generative adversarial network (GAN). With progressive upsampling, the difficulty of learning large-scale factors was reduced, and the spread of feature information between layers was enhanced by dense connection, which effectively solved the problem of gradient dispersion. In this research, it was mentioned that the Markov discriminator used in the Laplace algorithm can quickly construct a result matrix from the input data. During the training process, the generator was guided to pay attention to the local features of the image, thereby enriching the details of the reconstructed image. In summary, various image reconstructions and image optimizations based on the Laplace algorithm have very good application effects and have broad research prospects in the future.

5. Conclusion

In this study, an improved Laplace algorithm was designed for the QSM technique and applied to the QSM image analysis of 24 patients with PD in the experimental group. The results showed that QSM based on improved Laplace algorithm had a high diagnostic accuracy in the diagnosis of PD, showing a great adoption prospect. However, the selection of patient samples in this study was small and the source was single, which made it impossible to conduct a detailed discussion on the different features of QSM images of PD in this study or to verify the influence of these features on the diagnostic accuracy. In the future, increasing the sample size of PD patients and further adopting the multicenter cooperative analysis method for the study should be considered. In conclusion, the results provide a good theoretical basis for the adoption of Laplace-based improved QSM in the clinical diagnosis of PD.

Data Availability

The data used to support the findings of this study are available from the corresponding author upon request.

Conflicts of Interest

The authors declare no conflicts of interest.

Authors' Contributions

Guangxi Chen and Liang Zeng contributed equally to this work.

Acknowledgments

This work was supported by 2014 Wuhan Clinical Medical Research Project (WX14C16).

References

[1] Y. Wang, P. Spincemaille, Z. Liu et al., "Clinical quantitative susceptibility mapping (QSM): biometal imaging and its emerging roles in patient care," *Journal of Magnetic Resonance Imaging*, vol. 46, no. 4, pp. 951–971, 2017.

[2] J. Li, Y. Li, L. Gutierrez et al., "Imaging the centromedian thalamic nucleus using quantitative susceptibility mapping," *Frontiers in Human Neuroscience*, vol. 13, p. 447, 2020.

[3] S. Mazzucchi, D. Frosini, M. Costagli et al., "Quantitative susceptibility mapping in atypical Parkinsonisms," *NeuroImage: Clinic*, vol. 24, Article ID 101999, 2019.

[4] V. Shahmaei, F. Faeghi, A. Mohammadbeigi, H. Hashemi, and F. Ashrafi, "Evaluation of iron deposition in brain basal ganglia of patients with Parkinson's disease using quantitative susceptibility mapping," *European Journal of Radiology Open*, vol. 6, pp. 169–174, 2019.

[5] P. Saikiran and Priyanka, "Effectiveness of QSM over R2∗ in assessment of Parkinson's disease - a systematic review," *Neurology India*, vol. 68, no. 2, pp. 278–281, 2020.

[6] X. L. Liu, L. Q. Yang, F. T. Liu et al., "Short-echo-time magnitude image derived from quantitative susceptibility mapping could resemble neuromelanin-sensitive MRI image in substantia nigra," *BMC Neurology*, vol. 20, no. 1, p. 262, 2020.

[7] P. Ravanfar, S. M. Loi, W. T. Syeda et al., "Systematic review: quantitative susceptibility mapping (QSM) of brain iron profile in neurodegenerative diseases," *Frontiers in Neuroscience*, vol. 15, Article ID 618435, 2021.

[8] A. A. Joshi, C. Bhushan, R. Salloum, J. L. Wisnowski, D. W. Shattuck, and R. M. Leahy, "Using the anisotropic Laplace equation to compute cortical thickness," *Medical Image Computing and Computer Assisted Intervention - MICCAI 2018*, vol. 11072, pp. 549–556, 2018.

[9] B. Heim, F. Krismer, R. De Marzi, and K. Seppi, "Magnetic resonance imaging for the diagnosis of Parkinson's disease," *Journal of Neural Transmission*, vol. 124, no. 8, pp. 915–964, 2017.

[10] S. Lotankar, K. S. Prabhavalkar, and L. K. Bhatt, "Biomarkers for Parkinson's disease: recent advancement," *Neuroscience Bulletin*, vol. 33, no. 5, pp. 585–597, 2017.

[11] G. Pagano, F. Niccolini, and M. Politis, "Imaging in Parkinson's disease," *Clinical Medicine*, vol. 16, no. 4, pp. 371–375, 2016.

[12] N. Titova, C. Padmakumar, S. J. G. Lewis, and K. R. Chaudhuri, "Parkinson's: a syndrome rather than a disease?" *Journal of Neural Transmission*, vol. 124, no. 8, pp. 907–914, 2017.

[13] M. Fayyad, S. Salim, N. Majbour et al., "Parkinson's disease biomarkers based on α-synuclein," *Journal of Neurochemistry*, vol. 150, no. 5, pp. 626–636, 2019.

[14] D. B. Miller and J. P. O'Callaghan, "Biomarkers of Parkinson's disease: present and future," *Metabolism*, vol. 64, no. 3, pp. S40–S46, 2015.

[15] P. Mahlknecht, K. Seppi, and W. Poewe, "The concept of prodromal Parkinson's disease," *Journal of Parkinson's Disease*, vol. 5, no. 4, pp. 681–697, 2015.

[16] R. C. Helmich, D. E. Vaillancourt, and D. J. Brooks, "The future of brain imaging in Parkinson's disease," *Journal of Parkinson's Disease*, vol. 8, no. s1, pp. S47–S51, 2018.

[17] C. Atkinson-Clement, S. Pinto, A. Eusebio, and O. Coulon, "Diffusion tensor imaging in Parkinson's disease: review and meta-analysis," *NeuroImage: Clinic*, vol. 16, pp. 98–110, 2017.

[18] P. Borghammer and N. Van Den Berge, "Brain-first versus gut-first Parkinson's disease: a hypothesis," *Journal of Parkinson's Disease*, vol. 9, no. s2, pp. S281–S295, 2019.

[19] M. A. Nalls, C. Y. McLean, J. Rick et al., "Diagnosis of Parkinson's disease on the basis of clinical and genetic classification: a population-based modelling study," *The Lancet Neurology*, vol. 14, no. 10, pp. 1002–1009, 2015.

[20] X. Zou, H. Yu, and L. Zeng, "Laplace operator based reconstruction algorithm for truncated spiral cone beam computed tomography," *Journal of X-Ray Science and Technology*, vol. 21, no. 4, pp. 515–526, 2013.